Environmental
Science
Water Research & Technology

PAPER

View Article Online
View Journal | View Issue

Cite this: *Environ. Sci.: Water Res. Technol.*, 2023, **9**, 1502

Preparation and characterization of ZIF-8 and ZIF-67 engineered PVDF mixed-matrix membranes: stability enhancement in pervaporation study

Dipeshkumar D. Kachhadiya and Z. V. P. Murthy *

Received 19th January 2023,
Accepted 24th March 2023

DOI: 10.1039/d3ew00027c

rsc.li/es-water

In this work, mono-(ZIF-8 and ZIF-67) and bi-metallic (ZIF-8-67) metal–organic frameworks (MOFs) are prepared using the sol–gel method. The prepared MOFs are successfully applied to prepare mixed-matrix membranes. The prepared MOFs and MOF-incorporated mixed-matrix membranes are characterized by thickness and porosity, field-emission scanning electron microscopy with energy dispersive X-ray spectroscopy (FESEM-EDX), X-ray photoelectron spectroscopy (XPS), atomic force microscopy (AFM), Fourier transform infrared spectroscopy (FTIR), water contact angle, and X-ray diffraction (XRD) analysis. The performance evaluation of the prepared mixed-matrix membranes is carried out to study the effect of fillers, feed temperature, salt concentration, and stability of the membranes on the permeate flux and salt rejection. FESEM confirms the regular spherical shape of the nanoparticles. FTIR and XRD confirm the presence of the various functional groups and crystallinity of the nanofillers. The prepared mixed-matrix membranes are tested for desalination performance. It is observed that with an increase in temperature from 55 °C to 75 °C, the water flux increases for all the modified membranes with high salt rejection (>99%). The total flux of the prepared mixed-matrix membranes is enhanced when different ZIFs are incorporated into the pristine membrane. The total flux of M2, M3, and M4 varies from 34.1–96.5 L m^{-2} h^{-1}, 46.8–109.2 L m^{-2} h^{-1}, and 55.4–117.8 L m^{-2} h^{-1}, respectively. The M4 membrane has the highest water flux and salt rejection of 117.8 L m^{-2} h^{-1} and >99.6%, respectively. The long-term separation performance of the mixed-matrix membranes shows stable performance up to 220 h of the desalination experiment.

Water impact

Reverse osmosis (RO) is the most employed desalination process globally but this process is facing problems of higher operating pressure, low flux with time, and membrane fouling. As an alternative to RO, pervaporation can be a potential option for researchers because of its several advantages such as low operating pressure, no heavy piping required for the plant, and more fouling resistance compared to RO membranes for separating non-volatile components. This study shows the preparation of MOF based PVDF membranes and their desalination application using pervaporation.

Introduction

Freshwater is a necessity for all life on the planet. It is a critical feedstock in several major sectors, including food, petrochemicals, oil and gas, agriculture, electronics, and medicine.[1] Meeting the world's growing need for clean water poses enormous problems. The accessible freshwater supplies are diminishing due to the fast worldwide population expansion, global climate change, rapid industrialization, urbanization, and more rigorous health-based water quality requirements.[2] Numerous methods have been established to offer alternative water supplies *via* wastewater treatment, desalination, and recycling. These methods are membrane-based separation, ion exchange, distillation, and adsorption.[3] Among the many water treatment methods established, membrane-based separation has gained widespread acceptance owing to its excellent performance, cheap cost, and simplicity of operation.[4]

Reverse osmosis (RO) is the most employed desalination process globally, accounting for over 60% of all desalination facilities.[5,6] However, elevated operation pressure is needed to attain high osmotic pressure in RO treatment of high-salinity water, which makes it uneconomical.[5] Higher pressure, minimal water flux, and membrane fouling are the challenges with RO.[7] Recently, pervaporation (PV), a thermally driven process, succeeded as a viable desalination process because of its exceptional capacity to handle high-salinity water. Other advantages of PV are operating at low

---

Department of Chemical Engineering, Sardar Vallabhbhai National Institute of Technology, Surat – 395007, Gujarat, India. E-mail: ddkachhadiya@gmail.com, zvpm2000@yahoo.com, zvpm@ched.svnit.ac.in

pressure, no heavy piping required for the plant, and more fouling resistance compared to RO membranes for separating non-volatile components in contrast with membrane distillation (MD), which usually requires hydrophobic membranes. At the same time, PV uses hydrophilic water preferential dense membranes. Solar heating, geothermal energy, and waste energy may all be used to lower the cost of PV energy.[7] Thus, PV can be an excellent technique for desalination as an alternative to RO and MD, and developing a new hydrophilic membrane is the primary interest of scientists.[7] In PV, the water molecule transport mechanism through the membranes is according to solution–diffusion theory. Initially, water droplets are adsorbed on the top surface of mixed-matrix membranes at the feed side, diffuse across the membranes through mass transport nanochannels, and desorb at the permeate side of the membrane.[3]

Pervaporation membranes are made of polymers owing to their excellent selectivity, mechanical stability, ease of manufacturing and tunable transport properties. However, polymeric membranes have poor selectivity and chemical stability.[8] Various polymeric materials are available for membrane synthesis, such as PVDF, polyvinyl alcohol (PVA), polyetherimide (PEI), polyethersulfone (PSf), and polyether-*block*-amide (PEBA).[9,10] Developing novel membrane materials has sparked great interest in academics and businesses to improve the separation performance and blockage of different foulants.[11] As a result, preparing antifouling membranes for saltwater desalination has become a critical area of research.[12] Over the years, many techniques, materials, and modifications have been explored to develop antifouling polymeric membranes with improved flux and rejection performance.[13] Incorporating nanoparticles (NPs) in the polymer matrix is one of the well-established techniques to prepare such types of membranes. And the final prepared hybrid membrane is also known as a mixed-matrix membrane. Nanomaterials have been used to enhance the characteristics of conventional membranes (*e.g.*, flux, salt rejection, antifouling, stability, and antibacterial activity).[14] Various 2D nanomaterials, including graphene oxide (GO), silica-based materials (SiO_2), carbon nanotubes (CNTs), TiO_2, and zeolites, have been utilized as membrane fillers with promising results.[15] Nowadays, a new class of nanomaterials like metal–organic frameworks (MOFs) (UiOs, ZIFs, MILs, HKUSTs) are used as nanofillers for polymeric membranes. ZIFs are a subdivision of MOFs with a sodalite-like cage based on imidazole–metallic node bridging (*e.g.*, Zn, Co). In the production of ZIFs, a systematic combination of two metal ions and linkers leads to materials with a wide range of pore diameters and interface regions, providing potential alternatives. Aside from their remarkable chemical stability and extensive structural variety, the organic components of ZIFs, which may also increase filler–polymer compatibility, are a distinct benefit of adding ZIFs over several nanomaterials.[16] In this study, mono (ZIF-8 and ZIF-67) and bimetallic (ZIF-8-67) MOFs are prepared using a conventional method. With their smooth and hydrophilic surface, ZIFs reduce resistance to mass transfer, making them ideal for rapid fluid transport. Their size, shape, persistent porosity, flexibility, and excellent chemical and thermal stability make them exceptional candidates for various membrane-based separation applications. We have applied these inorganic fillers to prepare mixed-matrix membranes for saltwater desalination. Some research findings are available on inorganic filler-based polymeric membranes for saltwater desalination. Liang *et al.*[17] prepared GO/PAN membranes *via* vacuum-driven filtration. The prepared membrane shows a total flux of 14.3 L m^{-2} h^{-1} with >99.8% salt rejection at 30 °C for 35 000 ppm of NaCl feed solution.[17] A 3D-GOF-based polymeric membrane exhibits a flux and salt removal of 11.4 L m^{-2} h^{-1} and 99.9% for 35 000 ppm seawater at 90 °C.[18] A 2 wt% graphene nanoplate-based PEBA membrane is also reported for pervaporative desalination. The reported nanohybrid membrane shows a permeate flux of 2.58 L m^{-2} h^{-1} with >99.94% salt rejection.[19] Zhang *et al.*[20] prepared a microporous La/Y-codoped organosilica-based hydrophilic membrane with a permeate flux of 10.3 L m^{-2} h^{-1} and nearly 100% salt rejection for 3.5 wt% of NaCl feed solution at 25 °C.[20] GO filled sodium alginate membranes are also tested for pervaporative desalination. The prepared 2 wt% GO-filled NaAlg membranes exhibit a water flux and salt removal of 8.11 L m^{-2} h^{-1} and 99.95%, respectively, at 60 °C.[21] Also, it is observed that the water flux obtained from the pervaporative desalination route is not as comparable to the flux obtained from the RO process. But at the same time, membrane fouling and pore blocking in the RO are higher, which can reduce the flux over a certain period. Based on the above findings, it is noticed that the major challenge in front of researchers is to prepare highly stable polymeric membranes with high water flux and salt removal. Therefore, the present study aims to prepare highly stable and uniform structure-based mixed-matrix membranes using MOFs incorporated in PVDF membranes for pervaporative desalination. Researchers have recently focused on using mixed matrix membranes (MMMs) for this process, particularly those based on MOFs. Here are some of the potential merits of using MOF-based MMMs for pervaporative desalination: (1) enhanced permeability: adding MOFs to polymer matrices can enhance the permeability of the resulting MMMs, increasing the pervaporation process efficiency; (2) highly water-selective membrane: MOFs are known for their high selectivity for certain molecules due to their unique pore structure and chemical properties. By incorporating MOFs into MMMs, researchers can design membranes with high selectivity for water molecules over salt ions. This leads to the efficient separation of freshwater from seawater or brackish water; (3) stability: MOFs are stable under various conditions, including high temperatures and pressures, making them suitable for harsh environments. Incorporating MOFs into MMMs can enhance the stability of the resulting membranes, leading to longer membrane lifetimes and lower maintenance costs; and (4) tunability: MOFs can be synthesized with a wide range of pore sizes and surface chemistries, allowing researchers to tailor the properties of MMMs for specific applications. This means that MOF-based MMMs can be designed to optimize water separation from different feed streams, such as seawater or brackish water.

To the knowledge of the authors, no research has been found on pervaporative desalination using ZIF-8-67/PVDF mixed-matrix membranes. To prepare the highly stable and porous mixed-matrix membranes, the following are the objectives for this research work: (1) preparation of ZIF-8, ZIF-67, and ZIF-8-67; (2) preparation of the mixed-matrix membranes; (3) characterization of the MOFs and mixed-matrix membranes; (4) separation performance of the MOF-based PVDF mixed-matrix membranes; and (5) theoretical data generation based on molecular diffusion flow theory. Based on the objectives mentioned above, the present study focuses on synthesising ZIF-8, ZIF-67 and ZIF-8-67 MOFs, applying the same in PVDF membranes and preparing highly stable homogeneous microstructure based PVDF mixed matrix membranes for the desalination using the pervaporation route.

Experimental

Materials and chemicals

PVDF (average M_w = 180 000 by GPC, density = 1.78 g mL^{-1}), procured from Aldrich, India, is used to prepare a thin polymeric membrane layer. DI water is prepared using a Merck Millipore (Model: Elix Essential 10, France) setup. PEG200 (density = 1.12 g mL^{-1}, average M_w = 190–210), zinc salt ($Zn(NO_3)_2 \cdot 6H_2O$), 2-methylimidazole (2-MeIM) ($C_4H_6N_2$), cobalt salt ($Co(NO_3)_2 \cdot 6H_2O$), *N*,*N*-dimethylformamide (DMF) (density = 0.948 g mL^{-1}), acetone (density = 0.784 g mL^{-1}), and sodium chloride (NaCl) are purchased from Finar, India.

Instruments used for characterization

FE-SEM analysis is performed using a Nova Nano, FESEM 450. Before FESEM analysis, the samples are gold coated using a Quorum@150TES coater. The XRD analysis of the MOFs and mixed-matrix membranes is carried out using a Rigaku Miniflex. FTIR analysis is performed using a Spectrum GX, Perkin Elmer instrument. AFM analysis is performed using a NanoScope IV controller (Veeco Metrology Group). XPS analysis is performed using a Thermo Fisher Scientific ESCALAB250, USA. Thermogravimetric analysis (TGA) is performed using a Pyris-1, Perkin Elmer instrument. A goniometer 15EC-OCA measuring 270, DataPhysics is used to measure the contact angle of the mixed matrix membranes.

Synthesis of ZIF-8, ZIF-67, and ZIF-8-67

Mono-metallic MOFs (Zn salt-based ZIF-8 and cobalt salt-based ZIF-67) are synthesized as described in our previous work.[22] For bi-metallic ZIF-8-67, $Zn(NO_3)_2 \cdot 6H_2O$ (2.932 g) and $Co(NO_3)_2 \cdot 6H_2O$ (3.880 g) in 200 mL of methanol separately and 2-MeIM (13.055 g) are suspended separately in 400 mL of methanol. Further, a metal solution is poured into the linker solution dropwise under constant stirring. At 25 °C, both the solutions are mixed at 1000 rpm for an hour and allowed to crystallize for 24 h before being centrifuged (Model: C-24 plus REMI). This is followed by multiple rounds of washing of MOFs using methanol before separating them by centrifugation at a speed of 7000 rpm for 15 min and drying in a vacuum oven (Model: SHI-105, Shivam Lab Instruments) overnight at 70 °C.

Preparation of MOF-based PVDF mixed-matrix membranes

The mixed-matrix membranes are prepared using the non-solvent-induced phase inversion technique.[22,23] Dissolving 2 g of 15% PVDF and 1% PEG-200 in DMF (11.86 mL) at 55–65 °C with constant stirring at 100–110 rpm yields a homogeneous yellowish polymer dope solution. The optimum loading of MOFs into polymer dope solutions is selected based on a preliminary study shown in Table 1. The 15 wt% pure PVDF membrane is considered an unmodified membrane (M1). For the preparation of MOF-based PVDF membranes, 1.5 wt% of ZIF-8 (M2), 3 wt% of ZIF-67 (M3), and 2.5 wt% of ZIF-8-67 (M4) are added to the PVDF solution individually. Further, for the preparation of M1 to M4 membranes, the PVDF polymer, DMF solvent and MOFs have been used; these all are used in weight fraction (Table 2). Finally, the mixed-matrix membranes are prepared by casting the polymer dope solution on a horizontal plate using a film applicator. This is followed by dipping in a coagulation bath containing water as a non-solvent and drying under atmospheric conditions.[15,24] Further, the prepared membranes are cleaned and stored for experimental studies.

Characterization of MOFs and MOF membranes

FE-SEM is used to study the size and surface structure morphology of the MOFs and MOF-based PVDF mixed-matrix membranes, and the cross-section images of the prepared mixed-matrix membranes. Before the cross-section imaging analysis, the specimens are cut in liquid nitrogen under vacuum and coated with Au as a conducting material (gold coating thickness is 2–5 nm and coating cycle duration is around 20–25 s). FE-SEM with EDX is utilized to examine the MOF dispersion in the membranes. The crystalline structure and crystal phase of the prepared MOFs and PVDF mixed-matrix membranes are studied using XRD analysis. The chemical composition with different functional groups available in the synthesized MOFs and fabricated MOF-based PVDF mixed-matrix membranes is investigated using FTIR analysis at a wavelength of 400–4000 cm^{-1}. The AFM analysis is performed to study the surface roughness characteristics of the prepared MOF-based PVDF mixed-matrix membranes. To analyze the roughness of the prepared MOF-based mixed-matrix membranes, a dust-free 5 μm × 5 μm size sample is scanned using tapping mode at 1–5 Hz resonance frequency. The XPS analysis studies the functional groups and chemical composition of the prepared MOF-embedded PVDF mixed-

Table 1 Preliminary membrane dope composition, MOF weight percent, and water flux obtained for the membranes

Membrane	PVDF	Wt. of polymer	ZIF-8/ZIF-67/ZIF-8-67	Wt. of MOF	Time	Permeate volume		Total flux
	wt%	g	wt%	g	h	mL	L	L m^{-2} h
ZIF-8/PVDF	15	1.5	0.5	0.05	0.25	4.5	0.0045	28.63
	15	1.5	1.0	0.1	0.25	6.1	0.0061	38.82
	15	**1.5**	**1.5**	**0.15**	**0.25**	**9.5**	**0.0095**	**60.46**
	15	1.5	2.0	0.2	0.25	7.6	0.0076	48.36
ZIF-67/PVDF	15	1.5	1.0	0.1	0.25	6.3	0.0063	40.09
	15	1.5	2.0	0.2	0.25	8.5	0.0085	54.12
	15	**1.5**	**3.0**	**0.3**	**0.25**	**10.2**	**0.0102**	**64.18**
	15	1.5	4.0	0.5	0.25	9.3	0.0093	58.55
ZIF-8-67/PVDF	15	1.5	0.5	0.05	0.25	7.5	0.0075	47.73
	15	1.5	1.5	0.15	0.25	9.4	0.0094	59.82
	15	**1.5**	**2.5**	**0.25**	**0.25**	**12.5**	**0.0125**	**79.55**
	15	1.5	3.5	0.35	0.25	11.6	0.0116	73.82

matrix membranes with a monochromatic Al Kα X-ray source. TGA measures the thermal stability of the ZIF-67 nanoparticles and MMMs. TGA is performed in an aluminium pan with a 10–12 mg sample at 50–800 °C (heating rate: 30 °C min^{-1}) in a nitrogen environment (100 mL min^{-1}). A goniometer is used to investigate the wettability of the prepared MOF-based PVDF mixed-matrix membranes. As previously reported, the porosity of MOF-based PVDF mixed-matrix membranes is calculated using a gravimetric method.[24]

Pervaporative desalination experiments

For the experimental study, a lab-scale pervaporation setup is used. The experiments are performed using a flat sheet module with an effective membrane surface area of 6.285 cm^2. The feed solution is pre-heated before the experiment and kept constant during the experiment run by hot water circulation using a water bath. A four litre feed tank is connected to a circulating pump to pump the feed to the membrane module. The vacuum is maintained constant at the permeate side of the membrane module. After each experiment, a cold-water circulating condenser is applied to collect and measure the permeate volume at a specific time interval. A conductivity meter measures the conductivity of the feed and permeate solution (Thermo Fisher). Furthermore, the permeate flux (J_v) and salt rejection (R) of the mixed-matrix membranes are determined using eqn (1) and (2):

$$J_v = \frac{Q}{A \times T_i} \tag{1}$$

$$R = 1 - \frac{C_p}{C_f} \tag{2}$$

Table 2 Detailed composition of all four (M1 to M4) prepared membranes

Membrane	PVDF	PEG200	DMF	ZIF-8	ZIF-67	ZIF-8-67
M1	15	1	84.0	—	—	—
M2	15	1	82.5	1.5	—	—
M3	15	1	81.0	—	3	—
M4	15	1	82.0	—	—	2.5

where A = membrane area (m^2), Q = permeate volume (L), C_p and C_f = permeate and feed side salt concentrations, and T_i = time (h).

Theoretical model

A theoretical approach may learn about the process and the factors involved. It provides an understanding of how various process factors influence the performance of the membrane. The theoretical model for pervaporative desalination is evaluated using experimental data, and the accuracy of the experimental data is investigated. Some assumptions to develop the simulation model are as follows:

Steady-state flow on the feed side is assumed. The effect of concentration polarisation is negligible on the membrane surface. Vapour and liquid phases are in equilibrium on both sides of the membrane. No chemical reaction occurs on the feed side. For mass transfer across the membrane, the permeate flux of single component i, J_i can be written as eqn (3) and (4):[25]

$$J_i = B_i \times \Delta P_i = B_i \times (P_{w,f}{}^0 a_{w,f} - P_{w,p}{}^0 a_{w,p}) \tag{3}$$

$$J_i = B_i \times (P_{w,f}{}^0 \gamma_{w,f} x_{w,f} - P_{w,p}{}^0 \gamma_{w,p} x_{w,p}) \tag{4}$$

where J_i is the permeating flux of component 'i'; B_i is the membrane permeability; $P_{w,f}$ and $P_{w,p}$ are the partial water vapour pressure at the membrane feed and permeate sides, respectively. The membrane permeability mainly depends on temperature, pressure, thickness, pore size, and porosity. The partial vapour pressure of the mixture is a function of absolute temperature and solute mole fraction. It is calculated using eqn (5), and the pure water vapour pressure is given by the Antoine equation and calculated using eqn (6):

$$P_w(x, T) = P_w{}^0(T) a_w(x) \tag{5}$$

$$P_w{}^0(T) = \exp\left(23.1964 - \frac{3816.44}{T - 46.13}\right) \times 1.10325 \times \frac{10^5}{760} \tag{6}$$

For an aqueous mixture of NaCl, an empirical relationship between γ_w and the mole fraction of the solute is often used and calculated using eqn (7).[26] In contrast, the dilute aqueous stream is determined using eqn (8):

$$\gamma_w = 1 - 0.5x_{\mathrm{NaCl}} - 10x_{\mathrm{NaCl}}^2 \tag{7}$$

$$P_w(x_w, T) = (1 - x_s)P_w^0(T) \tag{8}$$

The kinetic gas theory is used to determine the membrane permeability. The molecular diffusion theory and Knudsen flow model suggest mechanisms for mass transfer across membranes.[27,28] The operating mechanism for a particular prepared mixed matrix membrane is effectively studied using the Knudsen number theory given in eqn (9). For the vapour phase water molecule, the free mean path (λ_w) is determined using the following eqn (10):[26]

$$K_n = \frac{\lambda_w}{d_p} \tag{9}$$

$$\lambda_w = \frac{K_b \times T}{\sqrt{2} \times \pi \times p_m \times (2.641 \times 10^{-10})^2} \tag{10}$$

where K_n is the Knudsen number; T is the temperature in K; P_m is the mean pore pressure and measured in Pa; d_p is the membrane pore size in m; K_b is the Boltzmann constant, and its value is 1.38064×10^{-24} J K^{-1}. If $K_n > 10$, the molecule–pore wall collision effect dominates over molecule–molecule collisions, then the Knudsen-type diffusion is applied, and the membrane permeability is calculated using eqn (11):[29]

$$B_i^k = \frac{2}{3RT} \times \frac{\varepsilon \bar{r}}{\tau \delta} \times \left(\frac{8RT}{\pi M_i}\right)^{\frac{1}{2}} \tag{11}$$

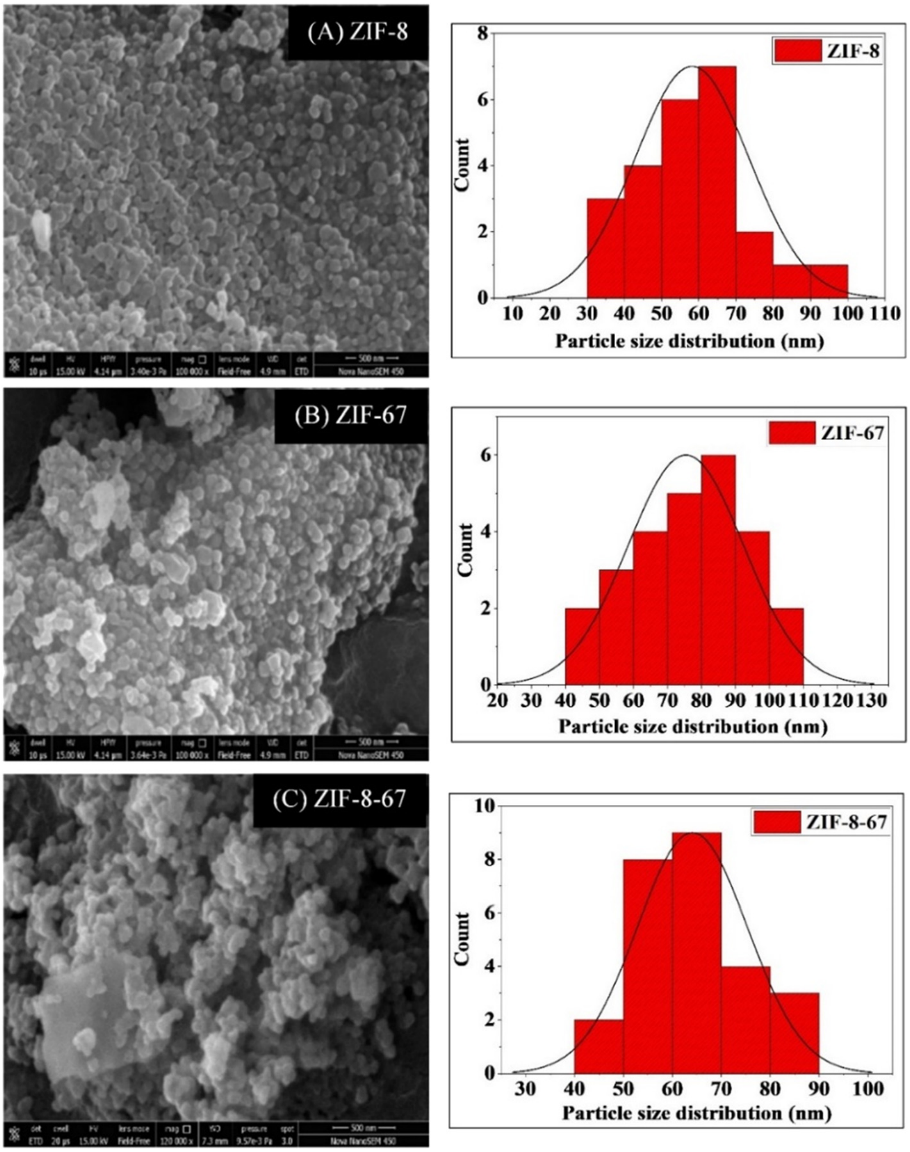

Fig. 1 FE-SEM images with particle size distribution: (A) ZIF-8, (B) ZIF-67, (C) ZIF-8-67.

If $0.01 < K_n < 10$, the water vapour transport occurs *via* a combined Knudsen/ordinary diffusion mechanism. In this case, the transition model is used to calculate the water vapour permeability of the membrane using eqn (12):

$$B_i^m = \frac{1}{RT\delta}\times\left(\frac{2\varepsilon\bar{r}}{3\tau}\left(\frac{8RT}{\pi M_i}\right)^{\frac{1}{2}}+\frac{\varepsilon\bar{r}^2}{8\tau\eta_i}\bar{P}\right) \qquad (12)$$

where $\bar{r}$ and δ are the mean pore radius and membrane thickness in meter (m); T is the absolute temperature in Kelvin (K); ε is the membrane porosity; M_i is the molecular wt of component 'i' in g mol^{-1}; τ is the tortuosity factor; η_i is the viscosity of component 'i'.

Results and discussion

MOF and membrane characterization

Fig. 1 presents the FESEM images of the ZIF-8, ZIF-67, and ZIF-8-67 MOFs. The surface morphology of ZIF-8 nanocrystals is shown in Fig. 1(A). In the present study, the FESEM images show that ZIF-8 has symmetrical and uniformly dispersed nano-sized spherical crystal morphologies, similar to the previously reported literature.[24] Fig. 1(B) presents the SEM image of the regular spherical crystal structure of ZIF-67 with a particle size of 76 ± 16 nm. The obtained data for ZIF-67 are well-matched with the previously reported study.[30] Fig. 1(C) presents the regular spherical ZIF-8-67 with a particle size of 65 ± 15 nm. Similar results are found in the previously published literature.[31,32] Fig. 2(A) shows the surface microstructure of all the prepared MOF-based PVDF mixed-matrix membranes (M1–M4), with several nanopores visible at the top surface. When pore-forming nano-additives are added to the pure PVDF polymer matrix, the surface morphology changes little compared to the M1 membrane. The FESEM images show the good compatibility of the MOFs in the polymer matrix, as observed on the top surface of the mixed-matrix membranes. It is observed that no cracks are found on the top surface of the MOF-modified mixed-matrix membranes, confirming the better dispersion and stability of the MOFs in the prepared mixed-matrix membranes. In

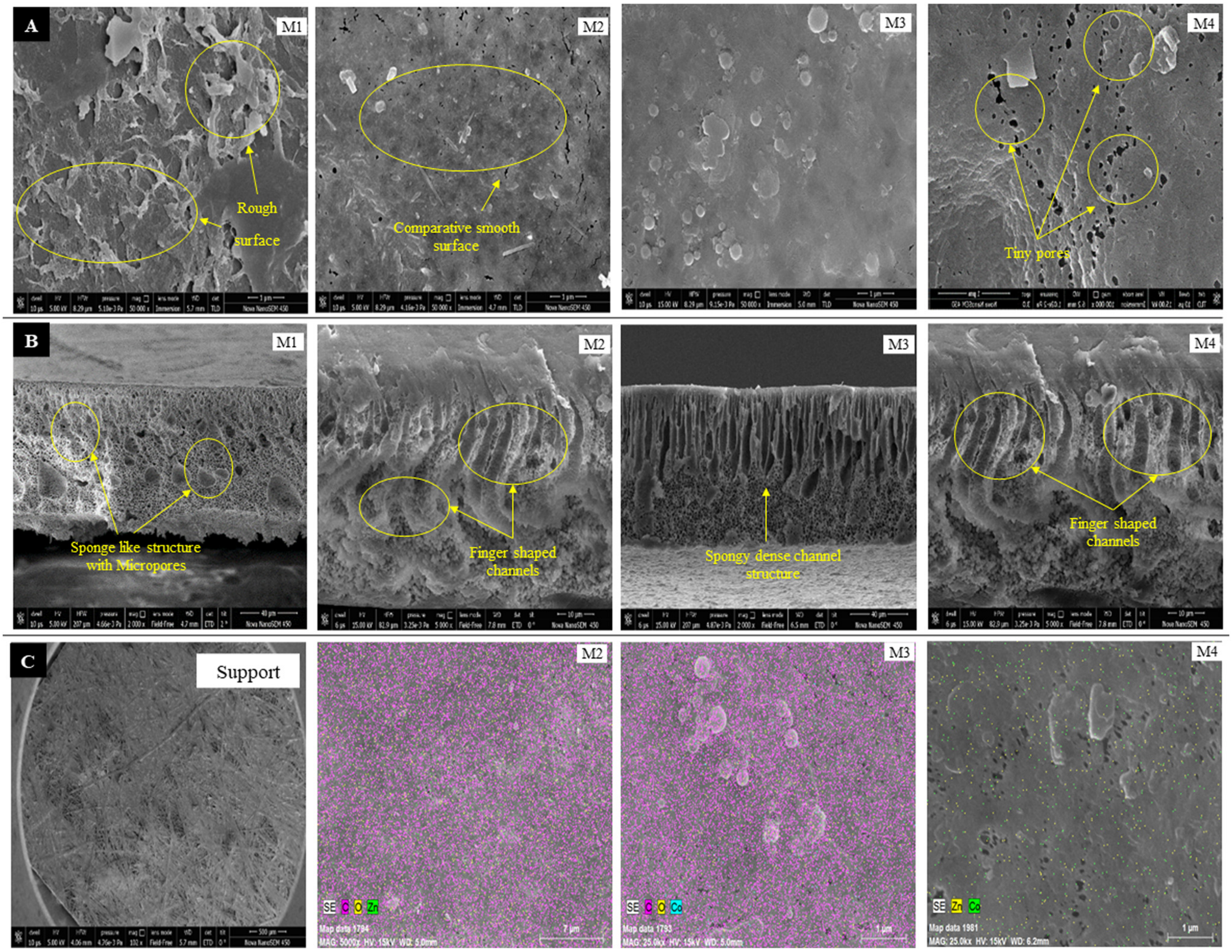

Fig. 2 FE-SEM images of the membranes: (A) surface images (M1 to M4), (B) cross-sectional images (M1 to M4), and (C) elemental mapping of M2, M3, and M4 mixed-matrix membranes.

comparison, tiny pores are found on the surface of M4. The synthesized membranes exhibit an uneven structure with channel-type regular micropores with dense spongy layers, as shown in Fig. 2(B). The diffusion rate between the solvent and non-solvent increases due to the presence of additives, forming bigger pores or channels in the membranes.[33] Compared to the pristine membrane, all the MOF-based mixed-matrix membranes show more porous structures (see Table 3). PEG-200 performs a vital role as a pore-forming agent, enabling the membrane pore distribution. PEG molecules can pass to the lean polymer phase of the membrane surface in conjunction with solvent outflow, so aggregated PEG molecules spread uniformly on the top surface of the membrane. Also, they increase the hydrophilicity of the membrane. ZIFs and their prepared derivative-based mixed-matrix membranes allow water molecules to pass through the membrane and block solutes, resulting in high water flux and salt rejection.[34] The dispersion of ZIF and its prepared derivatives in the polymeric matrix is investigated using elemental analysis as shown in Fig. 2(C). As shown in Fig. 2(C), homogeneous dispersion of the prepared MOFs is observed for all the mixed-matrix membranes. Most MOF particles are dispersed uniformly on the prepared membrane surface, but particle agglomeration is also found in some places because of their high concentration.

AFM is carried out to investigate the roughness and dispersion of nanoparticles in the polymeric membranes. The 2D and 3D AFM surface images of all four MOF-based PVDF mixed-matrix membranes (M1–M4) are presented in Fig. 3. Different surface parameters, such as root mean square data (R_q) and average surface roughness (R_a), are listed in Table 3. The brighter and darker points describe the highest peaks and lowest valleys of the surface topology of the mixed-matrix membranes in the 3D surface image. The M1 membrane has a smooth surface, with an R_a value of 12.3 nm compared to the other membranes. From Table 3, it is clear that incorporating MOFs into the polymeric membranes increases surface roughness.[35] The surface roughness of the prepared MOF-based PVDF mixed-matrix membranes depends on the water and DMF diffusion rate during the phase inversion process of the membranes. Incorporating hydrophilic MOFs and their derivatives into the polymeric membrane enhances the transfer rate of DMF and water in the water coagulation bath, which increases the roughness of the MOF-based PVDF mixed-matrix membranes. As the surface roughness increases, it provides a larger surface area; increased relative water permeability is also observed.[24,36] The R_a value increases with the loading of MOFs into the PVDF membranes. The R_a value of the MOF-based PVDF mixed-matrix membranes is 12.3 nm (M1), 13.1 nm (M2), 14.9 nm (M3), and 15.3 nm (M4).

Table 3 Porosity, thickness, and roughness characteristics of the prepared membranes

Membranes	Porosity (%)	Thickness (μm)	R_a (nm)	R_q (nm)
M1	22.1 ± 2.9	132 ± 4	12.3	18.3
M2	33.7 ± 0.9	149 ± 5	13.1	18.8
M3	37.7 ± 1.2	198 ± 5	14.9	20.5
M4	48.5 ± 3.9	139 ± 6	15.3	20.8

Fig. 4A presents the characteristic peaks using XRD analysis for the prepared different MOFs. The major peaks and planes of the ZIF-8 MOF are observed at 2θ of 7.38° (011), 10.08° (002), 12.78° (112), 14.72° (022), 16.50° (013), 18.08° (222), and 22.18° (114). The obtained characteristic peaks and planes for the ZIF-8 MOF are similar to the reported values in the literature.[37–39] The obtained characteristic peaks and planes of ZIF-67 at 2θ of 7.56° (011), 10.18° (002), 12.84° (112), 14.80° (022), 16.65° (013), 18.2° (222), and 22.32° (114) are matched with the literature.[39,40] The characteristic peaks are slightly shifted to the right for ZIF-67 and ZIF-8-67 compared to ZIF-8, which may be because the Zn^{2+} ions are greater than the Co^{2+} ions. The XRD patterns of the prepared membranes (M1 to M4) are shown in Fig. 4(B). The characteristic peaks and planes at 7.40° (011), 15.64° (022), 18.52° (222), 23.22° (233), 25.96° (224), 29.82° (044), 30.10° (334), and 31.50° (244) verify the presence of ZIF-8, ZIF-67, and ZIF-8-67 MOFs in the prepared mixed-matrix membranes.[41] In addition, the major peaks at 18.4°, 20.6° and 26.7° represent the α and β phases of PVDF.[42]

Fig. 4(C) presents the FTIR data of all the prepared MOFs. Significant bands at 3436 cm^{-1} (NH– residual of MeIM), 2923 cm^{-1} and 3137 cm^{-1} (aliphatic and aromatic C–H vibration of MeIM), 1458 cm^{-1} (entire ring stretching of MeIM), 1576 cm^{-1} and 1633 cm^{-1} (C═N stretching of MeIM), 992 cm^{-1}, 1302 cm^{-1}, and 1421 cm^{-1} (in-plane bending of MeIM), 684 cm^{-1} and 752 cm^{-1} (out-of-plane vibration of MeIM), 420 cm^{-1} (Zn–N vibration), and 424 cm^{-1} (Co–N stretching) are confirmed for all the samples. The results are matched with the previously reported literature.[43] Two characteristic peaks are seen at 1139 cm^{-1} and 1173 cm^{-1} according to the C–O stretching for MeIM. The FTIR curves of all four mixed-matrix membranes are given in Fig. 4D. The characteristic peaks at 1395 cm^{-1}, 1575 cm^{-1}, and 1307 cm^{-1} are related to C–N stretching, N–H bending, and C═N stretching vibration of the mixed-matrix membranes. The characteristics peaks at 2885 cm^{-1} (C–H vibration), 1720 cm^{-1} (C═O), and 1100 cm^{-1} (C–O vibration) confirm the presence of polyethylene glycol. Several peaks represent the core PVDF structure at 3021 cm^{-1} (asymmetric CH_2 vibration), 2991 cm^{-1} (symmetric CH_2 vibration), 1182 cm^{-1} (C–C vibration), and 840 cm^{-1} (C–F vibration). The characteristic peaks at 421 cm^{-1} and 425 cm^{-1} represent the Zn–N and Co–N stretching, showing that Zn and Co cations are bonded to the nitrogen atom of MeIM.[30,41]

The present study effectively incorporates different MOFs into PVDF membranes to enhance hydrophilicity and salt rejection. Hence after investigation, the water contact angle (WCA) of the pure PVDF membrane is found to be 81°. PVDF has a strong electronegative characteristic due to the

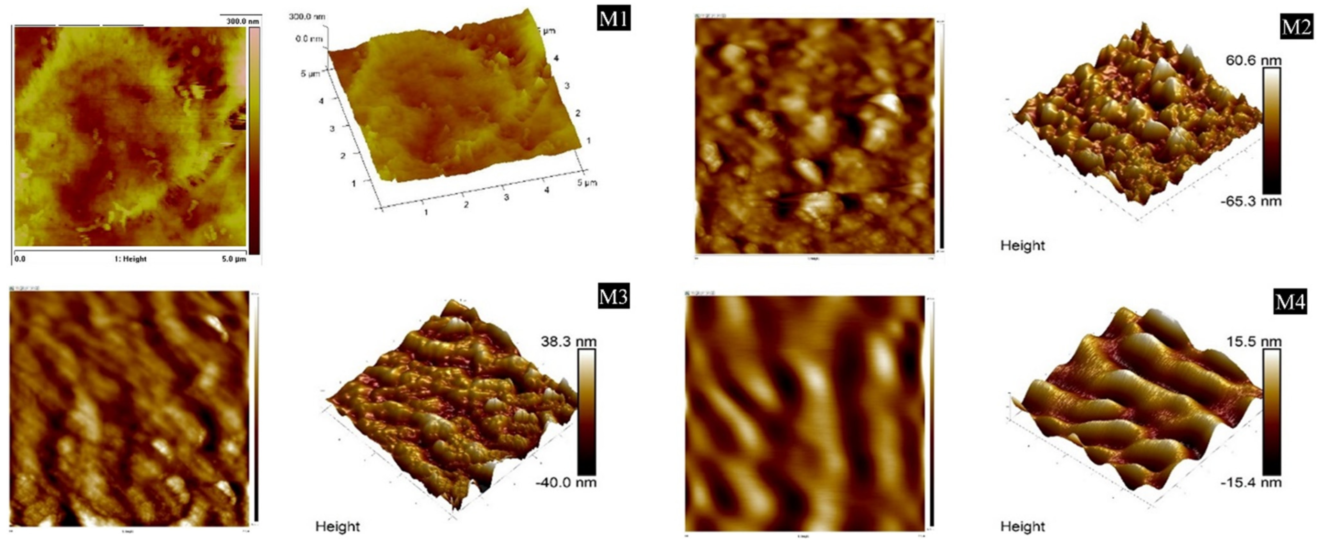

Fig. 3 The 2D and 3D surface images of the MOF-based PVDF mixed-matrix membranes.

presence of the $-CF_2$ molecule.[23] The fluorinated molecules of the PVDF matrix increase the WCA of the membrane. The membrane surface wetting qualities are critically dependent on van der Waals forces. The modified membranes have higher porosity and better pore distribution than the M1 membrane, allowing them to be more selective towards water. The van der Waals forces influence the surface-wetting features of the MOFs. The presence of OH-containing functional groups in the nanocrystals greatly improves the surface energy of the prepared mixed-matrix membranes.[24] The MOFs increase the membrane hydrophilicity, improving permeability and antifouling qualities. The water contact angles of the M2, M3, and M4 membranes decreased to 74°, 65°, and 53°, respectively, compared to the pristine membrane.

TGA is used to examine the percent weight loss of ZIF-8, ZIF-67, and ZIF-8-67 in the temperature range of room temperature to 850 °C with a N_2 flow (Fig. 4(E) and (F)). For ZIF-8 and ZIF-8-67, the weight loss is mainly due to the carbonization and decomposition of the metal and linker and it is observed in the temperature range of 450–650 °C. For ZIF-67, a two-stage weight loss is observed. First, the unreacted 2-MeIM and organic linker molecules from the cavities and surfaces of the MOFs are vaporized, resulting in a 26% weight loss at 260 °C. When the MOF precursor is heated over 385 °C, ZIF-67 carbonizes and decomposes, while ZIF-8 and ZIF-8-67 begin to decline at 540 and 600 °C, respectively. The residual amount left at 850 °C is 51%, 22%, and 54% for ZIF-8, ZIF-67, and ZIF-8-67, respectively. Here, in the enlarged view, one can see that the M1 membrane started deteriorating around the temperature range of ~400–420 °C. In contrast, the modified mixed matrix membranes (M2, M3 and M4) began decomposing after the temperature of ~460–510 °C. It is because of the formation of the H-bond due to the additives, which decreases the organic contents in the PVDF polymer matrix. The amounts of the residue obtained for the different membranes at 700 °C are 11.31% (M1), 17.30% (M2), 13.56% (M3), and 15.72% (M4).

The MOF-based PVDF mixed-matrix membranes are studied using XPS analysis and presented in Fig. 5. Substantial peaks are found at binding energies (BEs) of 285 eV (C1s), 396 eV (N1s), 530 eV (O1s), and 690 eV (F1s).[24,32] The N1s and O1s elements are found in the 2-MeIM linker and O–H functional group of the ZIFs. The high-resolution C1s peak, with four notable peaks found at 284.1 eV, 287.4 eV, 288.8 eV, and 290.5 eV binding energies, confirms the presence of C–C, C–N, C═O, and $-CF_2$, respectively. The presence of C–N bonds verifies the addition of the nitrogen group into the carbon network of the PVDF polymer film. The distinct peaks of the N1s spectra at binding energies of 400.3 eV, 399.1 eV, and 398.2 eV are related to graphitic N, pyrrolic N, and pyridinic N of 2-MeIM. At binding energies of 533.2 eV (O–C═O), 532.3 eV (C–O), and 531.5 eV (C=O), three notable peaks of the O1s spectra are found.[24] The dynamic shift of the C–F semi-ionic bond and covalent bond detected at 684 eV is connected to the F1s spectrum, which signified the α-phase orientation of PVDF. ZIF-8 and ZIF-67 are embedded in the PVDF membranes. The XPS characteristic peaks of Zn are present at binding energies between 1015 and 1045 eV. The present specific peaks of Zn $2P_{1/2}$ and Zn $2P_{3/2}$ are confirmed at 1021 eV and 1045 eV, respectively. Similarly, Co is present at binding energies between 770 to 810 eV, and the characteristic peaks of Co (Co $2P_{1/2}$ and Co $2P_{3/2}$) are confirmed at 781 eV and 797 eV.[44]

Experimental performance of the prepared MOF-based PVDF mixed-matrix membranes

Effect of different MOFs on water flux. Fig. 6 depicts the effect of different MOFs on the performance of the different MOF-based PVDF mixed-matrix membranes in the temperature range of 55 °C to 75 °C and at feed

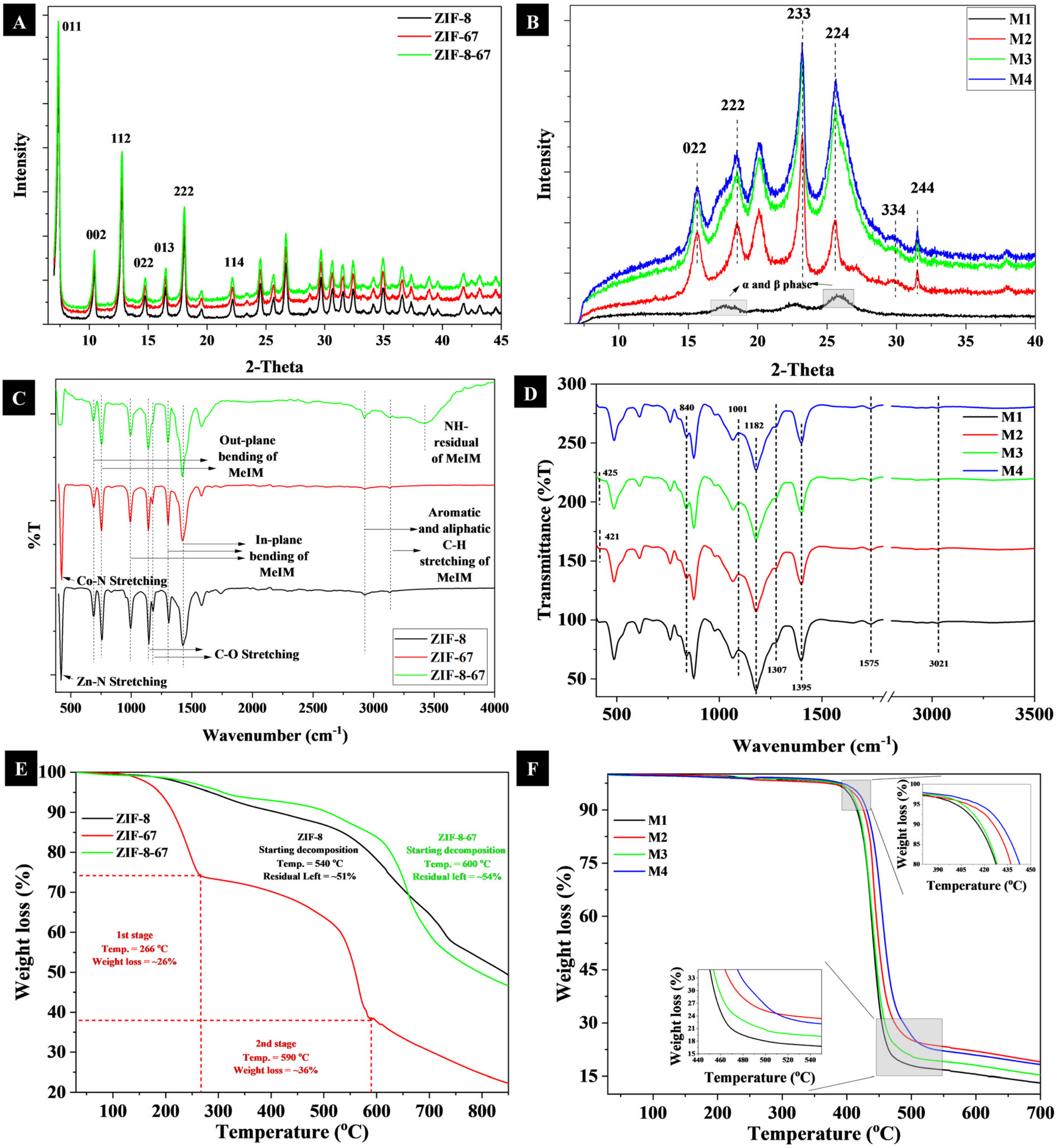

Fig. 4 (A and B) XRD patterns of the MOFs and membranes (M1 to M4), (C and D) FTIR spectra of the MOFs and membranes (M1 to M4), and (E and F) TGA analysis of the MOFs and membranes (M1 to M4).

concentrations of 1 wt% to 3.5 wt% of salt water using pervaporation. The pure water flux of the M1 membrane is 17.2 to 39.1 L m^{-2} h^{-1} at different operating temperatures. The total flux of the prepared mixed-matrix membranes is enhanced when different ZIFs are incorporated into the pristine membrane. The total flux of M2, M3, and M4 varies from 34.1–96.5 L m^{-2} h^{-1}, 46.8–109.2 L m^{-2} h^{-1}, and 55.4–117.8 L m^{-2} h^{-1}, respectively. When the ZIFs are incorporated into the PVDF solution, the membrane porosity increases, resulting in higher permeate flux in the prepared MOF-based PVDF mixed-matrix membranes. It enhances the channels and finger-like pores in the resulting membranes, which can help to enhance the permeate flux.

Effect of feed temperature and concentration on the flux and rejection. Fig. 7 presents the effect of feed concentration on the permeate flux and salt rejection for all four prepared membranes. When the amount of salt increases from 1 wt% to 3.5 wt%, the water flux decreases and the salt rejection increases across the board for all membranes. Theoretically, the salt present in water decreases the thermodynamic motion of water, thus reducing the driving force for separation. A higher feed solution concentration may also

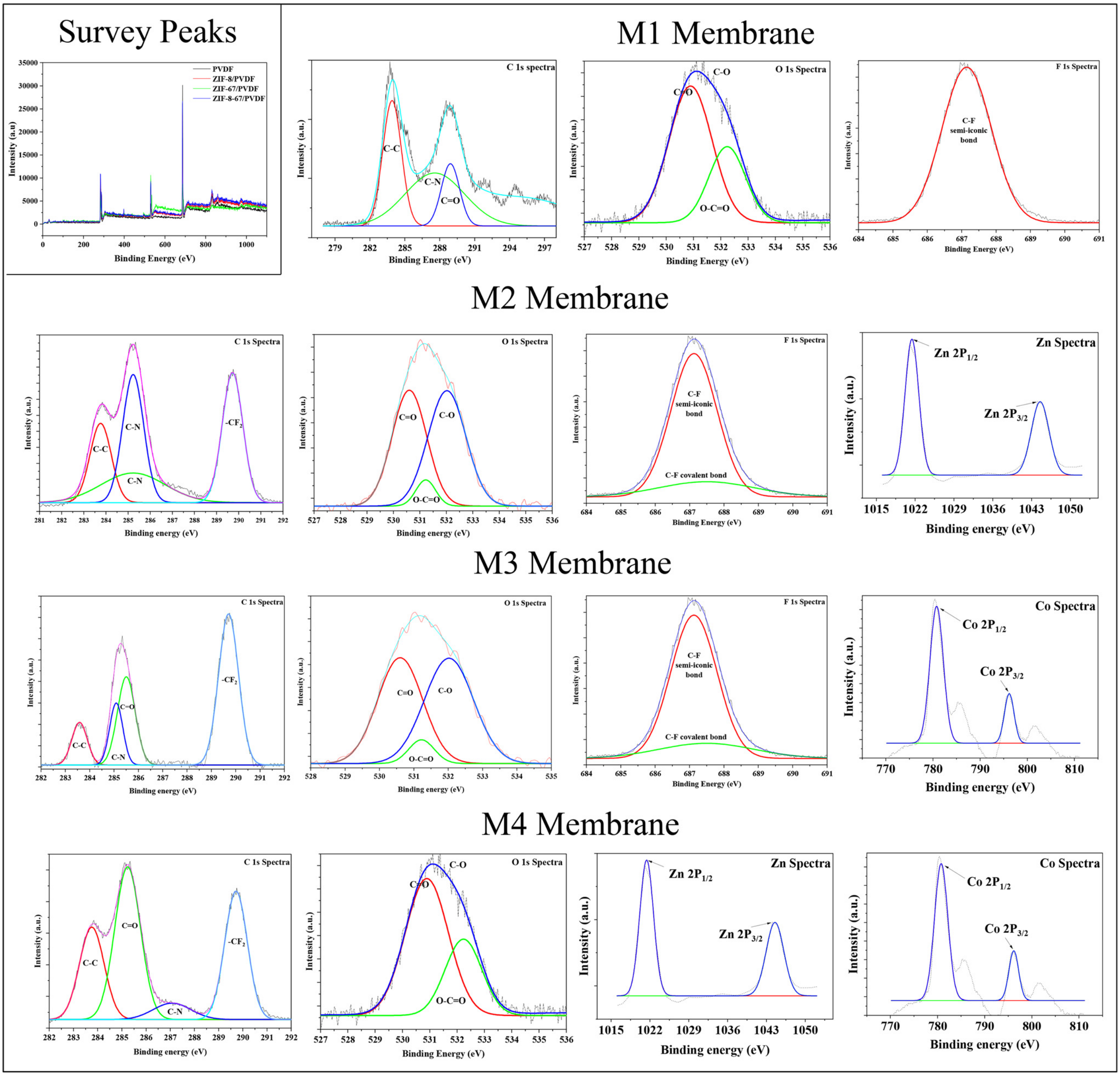

Fig. 5 XPS spectra of the prepared mixed-matrix membranes (M1 to M4).

result in concentration polarisation, reducing water flux.[45] The impact of feed composition on permeate flux is enhanced by raising the feed temperature since the water vapour pressure is exponentially related to the temperature.[46] A high feed concentration lowers the chain mobility of the membrane, resulting in reduced water flux. Therefore, it is noticed that the permeate flux decreases with increasing salt concentration for all four membranes.

Fig. 8 describes the water flux and salt removal as a function of feed temperature for all the prepared membranes. Temperature is an essential parameter in membrane desalination *via* pervaporation. An increase in temperature directly affects the solubility and diffusivity of water in the mixed-matrix membranes. As the temperature increases, the thermal motion of the polymeric chain increases, which increases the diffusion rate in the polymer. Due to the high thermal movement of the membrane chain, water molecules can quickly pass through it, resulting in high water flux. From Fig. 8, the impact of salt concentration on permeate flux is improved by raising the feed temperature since the water vapour pressure is exponentially proportional to the temperature.[45] Increasing the feed temperature increases water permeability, allowing water molecules to pass more readily across the membrane.[47]

Membrane stability test. For practical desalination applications, the long-term stability of mixed-matrix membranes is critical. Therefore, the experiments are performed for 220 h at 75 °C for all four (M1–M4) prepared

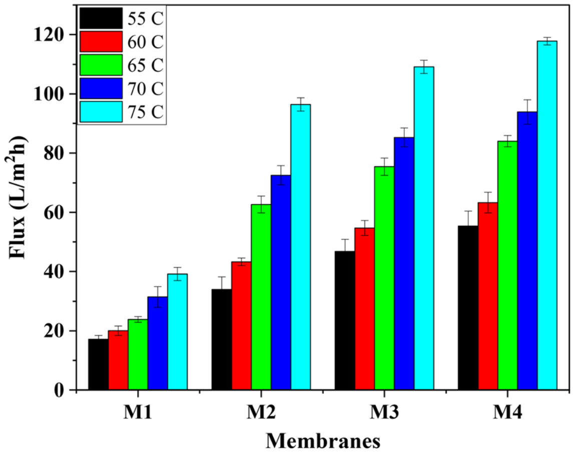

Fig. 6 Effect of different MOFs on the membrane water flux performance.

MOF-based PVDF mixed-matrix membranes for 3.5 wt% saltwater. Fig. 9 depicts the good stability of the synthesized MOF membranes with continuous water flux with high salt rejection. As indicated before, as the experimental duration increases, the water flux decreases, but the salt removal remains steady. One explanation for the drop in water flux over time is salt deposition on the active surface, which will block the pores of the prepared mixed-matrix membranes and increase mass transfer resistance, reducing water flux.

Performance comparison with the available literature. Several studies have described various membranes and their performance in pervaporation desalination (Table 4). It is observed that the prepared hydrophilic mixed-matrix membranes exhibited reasonable flux, salt rejection and stability performance compared to other reported studies.

Theoretical performance evaluation. The modelling data are generated for pure water and NaCl feed aqueous solution (1–3.5 wt%) at 55–75 °C and vacuum pressure ranging from 500 to 650 mmHg with a 110–140 μm thick PVDF flat sheet membrane. Four parameters (feed temperature, feed concentration, permeate side pressure, and membrane thickness) are considered for model predictions. First, the feed temperature is an essential parameter for saltwater desalination, directly affecting the permeate flux. As the feed

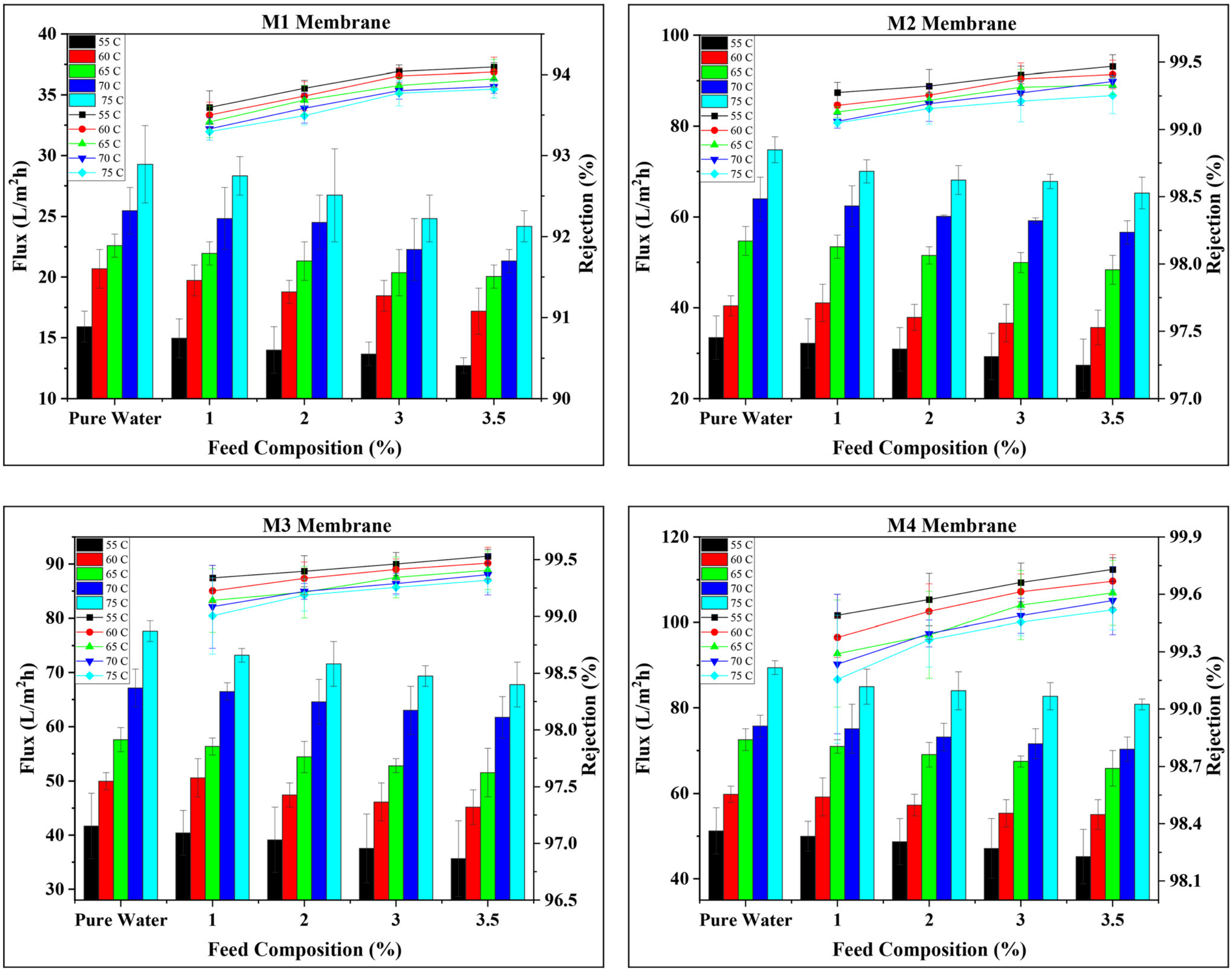

Fig. 7 Effect of feed concentration on water flux and salt rejection for M1 to M4 membranes.

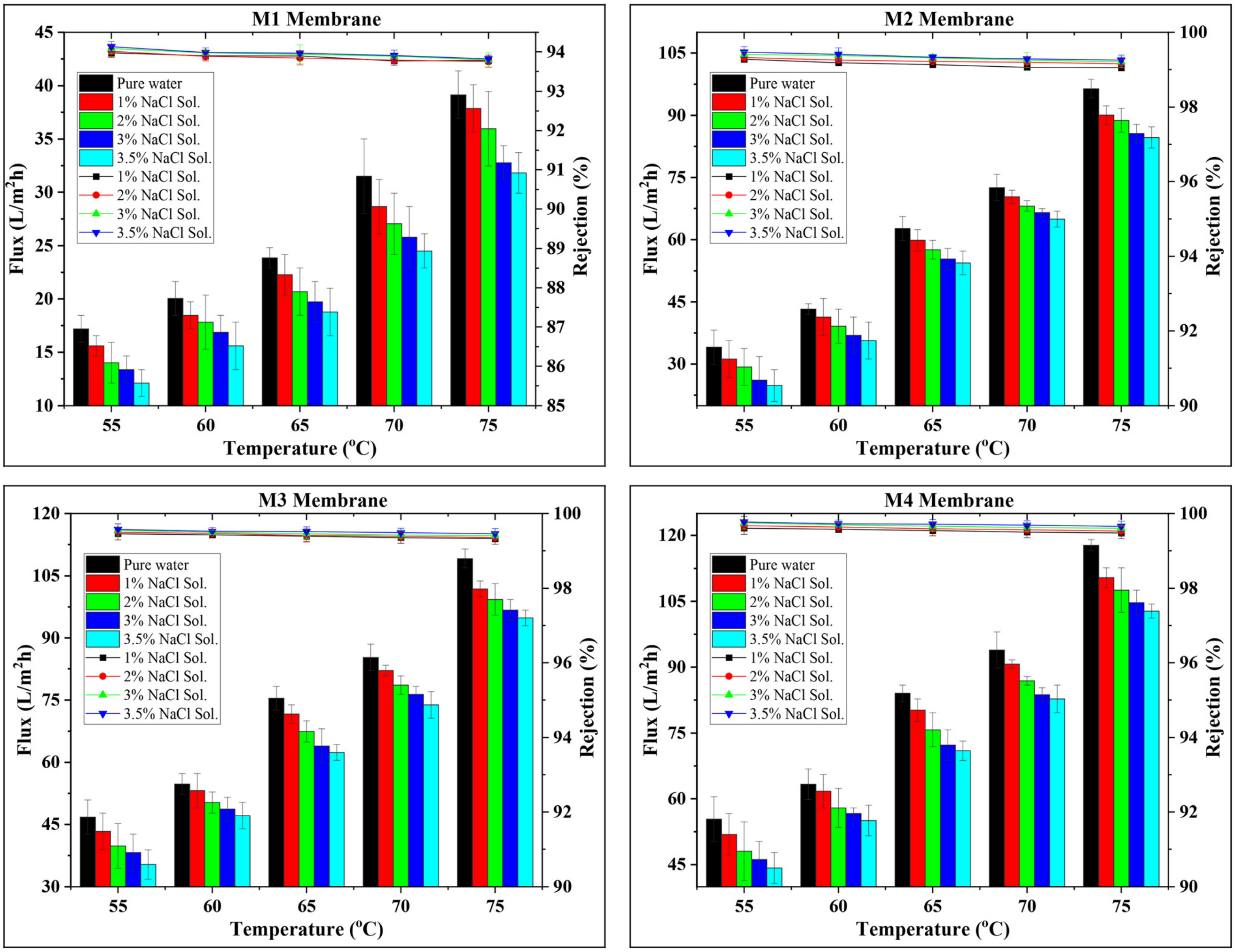

Fig. 8 Effect of feed temperature on water flux and salt rejection for M1 to M4 membranes.

temperature increases, the permeate flow exponentially increases. The model predictions and actual results for water flux with feed temperature using a PVDF flat sheet membrane configured as described in Table 5 are shown in Fig. 10. The higher water permeate flux observed at high temperatures may be due to membrane pore wetting and high energy consumption at higher operating feed temperatures. Increased water flux is achieved by increasing the feed temperature while keeping the feed flow rate and permeate side vacuum constant. The feed concentration is important for separating valuable components from an aqueous solution. The permeate flux reduces as the concentration of non-volatile solutes in the feed mixture increases, owing to the reduced water vapour pressure caused by the solutes added to water (eqn (5) and (6)). As the salt concentration in the feed increases, the permeate flux decreases, leading to the concentration polarisation effect, further resulting in membrane scaling (Fig. 10(B)). Third, the permeate side pressure is an important parameter for saltwater desalination performance. As the permeate side pressure increases, the permeate flux decreases slightly. It is observed from Fig. 10(C) that there is no such effect of vacuum on the permeate flux. However, the permeate side

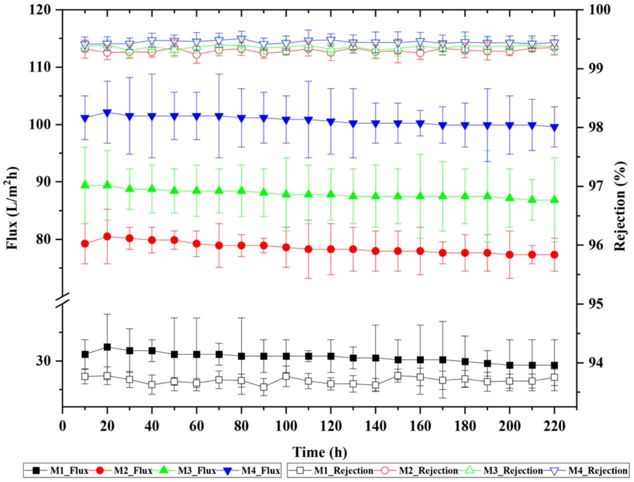

Fig. 9 Stability performance of the prepared membranes (M1 to M4) for 3.5 wt% of salt water for 220 h at 75 °C.

Table 4 Comparison of saltwater desalination by pervaporation with different reported studies

Membrane	Feed conc. (ppm)	Effective surface area (cm^2)	Temp. (°C)	Flux (L m^{-2} h^{-1})	Rejection (%)	Stability (h)	Ref.
MWCNT/PVA	35 000	12.6	22	6.96	99.9	30	16
GO/PAN	35 000	14.7	30	14.3	>99.8	—	17
GOF/PAN	35 000	—	90	11.4	>99.9	120	18
Graphene nanoplates/PEBA	35 000	19.625	35	2.58	99.94	60	19
$La_{25}Y_{75}SiO_2$	35 000	24	25	10.3	100	200	20
Alg-GO	35 000	19.6	60	8.11	99.41	—	21
Cellulose triacetate/CNCs	30 000	19.625	70	11.67	99.7	—	48
PVA green silica	35 000	50	60	12.3	99.9	—	49
Sulfonated polyether-ether ketone on PES	10 000	30	70	6.45	99.84	50	50
	30 000			6.13	99.94		
	70 000			5.73	99.99		
	100 000			4.98	99.97		
ZIF-8/PVDF	35 000	6.285	75	79.23	99.3	220	This study
ZIF-67/PVDF				89.41	99.4		
ZIF-8-67/PVDF				117.8	99.6		

Table 5 The typical input parameters and membrane configuration data for the model

Membrane	Feed temperature (°C)	Porosity	Membrane thickness (μm)	Pore diameter (μm)	Tortuosity factor (τ)	Permeate side pressure (mmHg)
PVDF	55–75	0.18	110–140	0.45	2.12	500–650

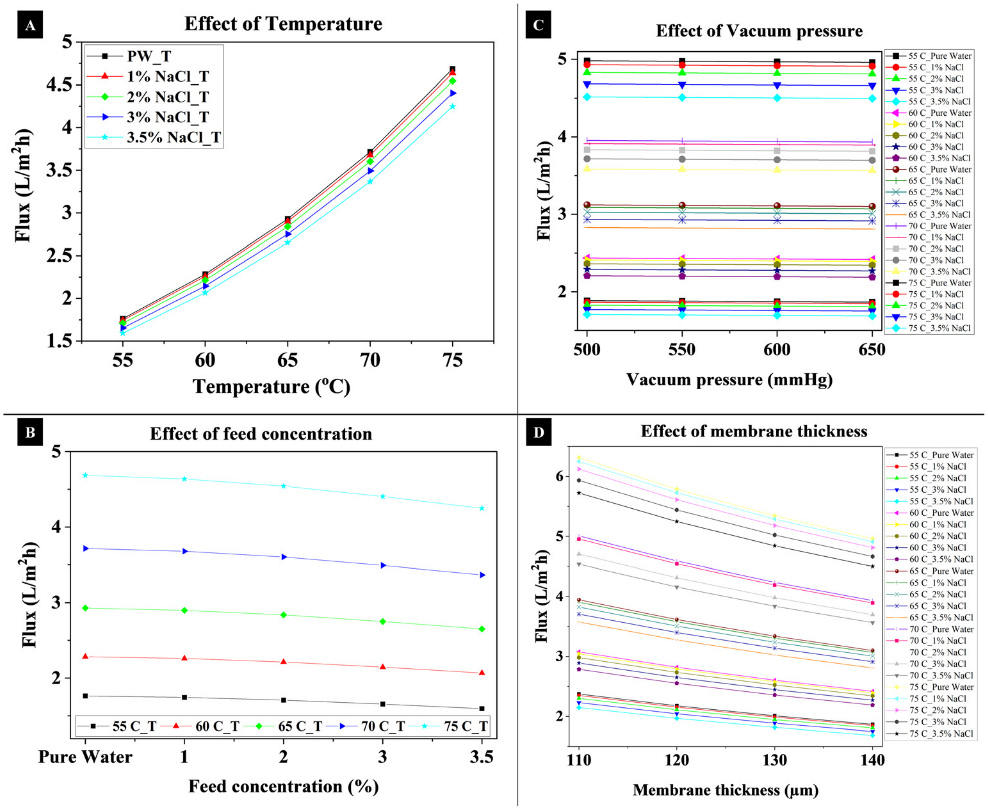

Fig. 10 Modelling data: (A) feed temperature *vs.* flux, (B) feed concentration *vs.* flux, (C) vacuum pressure *vs.* flux, and (D) membrane thickness *vs.* flux.

pressure separates volatile solutes from the aqueous mixture. Fourth, the thickness of the polymeric membranes plays a crucial role in the permeate flux for membrane-based separation. The prediction trend of total flux as a function of membrane thickness is shown in Fig. 10(D). A thinner membrane reduces the mass transfer barrier to permeate flux, resulting in increased permeate flux. Simultaneously, the temperature difference across the membrane decreases, resulting in a reduction in permeate flow. Therefore, an optimum membrane thickness is important for optimized performance.[51]

Conclusions

This study uses ZIFs and their derivatives as nanofillers to pure PVDF membranes for pervaporative saltwater desalination. All four (M1–M4) mixed-matrix membranes are synthesized using a phase inversion technique. The experiments are performed using three different MOF-based PVDF mixed-matrix membranes (PVDF, ZIF-8/PVDF, ZIF-67/PVDF, and ZIF-8-67/PVDF) at different temperatures (55 °C to 75 °C) and feed compositions (1 wt% to 3.5 wt%). By incorporating ZIFs into a pure PVDF membrane, the hydrophilicity and porosity of the membranes are increased, resulting in an improvement in the membrane separation performance. The experimental findings indicate that the feed concentration and temperature considerably impact the total flux but have a minor effect on the salt rejection. Among all four membranes, the M4 membrane has the maximum water flux of 117.8 ± 3.8 L m^{-2} h^{-1} and >99.6 ± 0.1% salt rejection. All the synthesized mixed-matrix membrane membranes exhibit excellent performance for a 220 h separation experiment. The experimental findings show that mono- and bimetallic MOFs may be useful for fabricating pervaporative desalination mixed-matrix membranes with high pure water flux and salt rejection.

Data availability

The data that support the findings of this study are available from the corresponding author upon reasonable request.

Author contributions

Dipeshkumar D. Kachhadiya: conceptualization, methodology, software, validation, formal analysis, investigation, writing – review & editing. Z. V. P. Murthy: corresponding author, supervision, conceptualization, methodology, resources, writing – review & editing, data curation, project administration.

Conflicts of interest

The authors declare that they have no known competing financial interests or personal relationships that could have appeared to influence the work reported in this paper.

Acknowledgements

The first author (DDK) acknowledges the Ministry of Education, Government of India, for a doctoral fellowship. The authors acknowledge the Material Research Center (MRC), MNIT Jaipur (India), the Sophisticated Analytical Instrument Facility (SAIF), IIT Bombay (India) and FIST (Physics)–IRCC SPM Central Facility of IIT Bombay for providing characterization facilities. Also, the authors acknowledge the Association for Harnessing Innovation and Entrepreneurship (ASHINE), SVNIT, Surat, for providing partial financial support.

References

1 Y. H. Teow and A. W. Mohammad, New generation nanomaterials for water desalination: A review, *Desalination*, 2019, **451**, 2–17, DOI: **10.1016/j.desal.2017.11.041**.

2 K. Berijani, A. Morsali and H. Garcia, Synthetic strategies to obtain MOFs and related solids with multimodal pores, *Microporous Mesoporous Mater.*, 2023, **349**, 112410, DOI: **10.1016/j.micromeso.2022.112410**.

3 Y. K. Ong, G. M. Shi, N. L. Le, Y. P. Tang, J. Zuo, S. P. Nunes and T. S. Chung, Recent membrane development for pervaporation processes, *Prog. Polym. Sci.*, 2016, **57**, 1–31, DOI: **10.1016/j.progpolymsci.2016.02.003**.

4 M. Yao, L. D. Tijing, G. Naidu, S. Kim, H. Matsuyama, A. Fane and H. Shon, A review of membrane wettability for the treatment of saline water deploying membrane distillation, *Desalination*, 2020, **479**, 114312, DOI: **10.1016/j.desal.2020.114312**.

5 G. Genduso, A. Missinne, Z. Ali, W. Ogieglo, B. Van der Bruggen and I. Pinnau, Hydrophobic polydimethylsiloxane thin-film composite membranes for the efficient pervaporative desalination of seawater and brines, *Sep. Purif. Technol.*, 2022, **280**, 119819, DOI: **10.1016/j.seppur.2021.119819**.

6 J. Sun, X. Qian, Z. Wang, F. Zeng, H. Bai and N. Li, Tailoring the microstructure of poly(vinyl alcohol)-intercalated graphene oxide membranes for enhanced desalination performance of high-salinity water by pervaporation, *J. Membr. Sci.*, 2020, **599**, 117838, DOI: **10.1016/j.memsci.2020.117838**.

7 Y. Li, E. Thomas, M. Molina, S. Mann, W. Walker, M. Lind and F. Perreault, Desalination by membrane pervaporation: A review, *Desalination*, 2023, **547**, 116223, DOI: **10.1016/j.desal.2022.116223**.

8 X. Cheng, F. Pan, M. Wang, W. Li, Y. Song, G. Liu, H. Yang, B. Gao, H. Wu and Z. Jiang, Hybrid membranes for pervaporation separations, *J. Membr. Sci.*, 2017, **541**, 329–346, DOI: **10.1016/j.memsci.2017.07.009**.

9 A. V. Sonawane and Z. V. P. Murthy, Dairy industry wastewater treatment by MOF and 2D nanomaterial engineered PVDF membranes based aerobic MBR: Membrane fouling mitigation and stability study, *Process Saf. Environ. Prot.*, 2023, **171**, 680–693, DOI: **10.1016/j.psep.2023.01.062**.

10 A. V. Sonawane and Z. V. P. Murthy, Antibiotic removal by metal–organic framework and 2D nanomaterial based polyetherimide mixed matrix membranes using a membrane

bioreactor, *Environ. Sci.: Water Res. Technol.*, 2023, **9**, 86–103, DOI: **10.1039/D2EW00620K**.

11 C. Lavanya and R. Geetha Balakrishna, Naturally derived polysaccharides-modified PSF membranes: A potency in enriching the antifouling nature of membranes, *Sep. Purif. Technol.*, 2020, **230**, 115887, DOI: **10.1016/j.seppur.2019.115887**.

12 D. D. Kachhadiya and Z. V. P. Murthy, Graphene oxide modified CuBTC incorporated PVDF membranes for saltwater desalination via pervaporation, *Sep. Purif. Technol.*, 2022, **290**, 120888, DOI: **10.1016/j.seppur.2022.120888**.

13 A. Alkhouzaam and H. Qiblawey, Functional GO-based membranes for water treatment and desalination: Fabrication methods, performance and advantages. A review, *Chemosphere*, 2021, **274**, 129853, DOI: **10.1016/j.chemosphere.2021.129853**.

14 D. D. Kachhadiya and Z. V. P. Murthy, Highly efficient chitosan-based bio-polymeric membranes embedded with green solvent encapsulated MIL-53 (Fe) for methanol/MTBE separation by pervaporation, *J. Environ. Chem. Eng.*, 2023, **11**(2), 109307, DOI: **10.1016/j.jece.2023.109307**.

15 A. S. Reddy, S. Kalla and Z. V. P. Murthy, Nanoparticles enhanced hydrophobic membranes: High-performance study for dye wastewater treatment using membrane distillation, *J. Water Process. Eng.*, 2022, **46**, 102610, DOI: **10.1016/j.jwpe.2022.102610**.

16 G. Yang, Z. Xie, M. Cran, D. Ng and S. Gray, Enhanced desalination performance of poly (vinyl alcohol)/carbon nanotube composite pervaporation membranes via interfacial engineering, *J. Membr. Sci.*, 2019, **579**, 40–51, DOI: **10.1016/j.memsci.2019.02.034**.

17 B. Liang, W. Zhan, G. Qi, S. Lin, Q. Nan, Y. Liu, B. Cao and K. Pan, High performance graphene oxide/polyacrylonitrile composite pervaporation membranes for desalination applications, *J. Mater. Chem. A*, 2015, **3**, 5140–5147, DOI: **10.1039/C4TA06573E**.

18 B. Feng, K. Xu and A. Huang, Covalent synthesis of three-dimensional graphene oxide framework (GOF) membrane for seawater desalination, *Desalination*, 2016, **394**, 123–130, DOI: **10.1016/j.desal.2016.04.030**.

19 F. U. Nigiz, Preparation of high-performance graphene nanoplate incorporated polyether block amide membrane and application for seawater desalination, *Desalination*, 2018, 164–171, DOI: **10.1016/j.desal.2017.08.025**.

20 H. Zhang, J. Wen, Q. Shao, A. Yuan, H. Ren, F. Luo and X. Zhang, Fabrication of La/Y-codoped microporous organosilica membranes for high-performance pervaporation desalination, *J. Membr. Sci.*, 2019, **584**, 353–363, DOI: **10.1016/j.memsci.2019.05.023**.

21 F. U. Nigiz, Graphene oxide-sodium alginate membrane for seawater desalination through pervaporation, *Desalination*, 2020, **485**, 114465, DOI: **10.1016/j.desal.2020.114465**.

22 D. D. Kachhadiya and Z. V. P. Murthy, Preparation and characterization of ZIF-8 and ZIF-67 incorporated poly (vinylidene fluoride) membranes for pervaporative separation of methanol/water mixtures, *Mater. Today Chem.*, 2021, **22**, 100591, DOI: **10.1016/j.mtchem.2021.100591**.

23 D. D. Kachhadiya and Z. V. P. Murthy, Separation of n-butanol from aqueous mixtures using TiO_2 and h-BN functionalized MIL-101 (Cr) incorporated PVDF mixed matrix membranes, *Sep. Purif. Technol.*, 2023, **306**, 122613, DOI: **10.1016/j.seppur.2022.122613**.

24 A. V. Sonawane and Z. V. P. Murthy, Synthesis, characterization, and application of ZIF-8/Ag_3PO_4, MoS_2/Ag_3PO_4, and h-BN/Ag_3PO_4 based photocatalytic nanocomposite polyvinylidene fluoride mixed matrix membranes for effective removal of drimaren orange P2R, *J. Membr. Sci.*, 2022, **641**, 119939, DOI: **10.1016/j.memsci.2021.119939**.

25 K. W. Lawson and D. R. Lloyd, Membrane distillation, *J. Membr. Sci.*, 1997, **124**, 1–25, DOI: **10.1016/S0376-7388(96)00236-0**.

26 E. A. Mason and A. P. Malinauskas, *Gas transport in porous media: Dusty-gas model*, Chemical Engineering Monographs, Elsevier, 1983, vol. 17.

27 M. Khayet, M. P. Godino and J. I. Mengual, Modelling Transport Mechanism Through A Porous Partition, *J. Non-Equilib. Thermodyn.*, 2001, **26**, 1–14, DOI: **10.1515/JNETDY.2001.001**.

28 M. Khayet and T. Matsuura, Pervaporation and vacuum membrane distillation processes: Modeling and experiments, *AIChE J.*, 2004, **50**, 1697–1712, DOI: **10.1002/aic.10161**.

29 K. W. Lawson and D. R. Lloyd, Membrane distillation. I. Module design and performance evaluation using vacuum membrane distillation, *J. Membr. Sci.*, 1996, **120**, 111–121, DOI: **10.1016/0376-7388(96)00140-8**.

30 X. Li, Y. Qiao, C. Wang, T. Shen, X. Zhang, H. Wang, Y. Li and W. Gao, MOF-derived Co/C nanocomposites encapsulated by $Ni(OH)_2$ ultrathin nanosheets shell for high performance supercapacitors, *J. Alloys Compd.*, 2019, **770**, 803–812, DOI: **10.1016/j.jallcom.2018.08.164**.

31 J. Yang, F. Zhang, H. Lu, X. Hong, H. Jiang, Y. Wu and Y. Li, Hollow Zn/Co ZIF particles derived from core-shell ZIF-67@ZIF-8 as selective catalyst for the semi-hydrogenation of acetylene, *Angew. Chem., Int. Ed.*, 2015, **54**, 10889–10893, DOI: **10.1002/anie.201504242**.

32 D. Zhang, J. Zhang, M. Pan, Y. Wang and T. Sun, Necklace-like C-ZIF-8@MWCNTs fabricated by electrochemical deposition towards enhanced supercapacitor, *J. Alloys Compd.*, 2021, **853**, 157368, DOI: **10.1016/j.jallcom.2020.157368**.

33 A. Karimi, A. Khataee, V. Vatanpour and M. Safarpour, High-flux PVDF mixed matrix membranes embedded with size-controlled ZIF-8 nanoparticles, *Sep. Purif. Technol.*, 2019, **229**, 115838, DOI: **10.1016/j.seppur.2019.115838**.

34 E. Celik Madenli and Z. Ilkay Ciftci, Effects of the carbon nanotube and polymer amounts on ultrafiltration membranes, *Environ. Eng. Res.*, 2021, **27**, 210626, DOI: **10.4491/eer.2021.626**.

35 L. J. Liu, G. E. Chen, H. F. Mao, Y. Wang and J. J. Wan, High performance polyvinylidene fluoride (PVDF) mixed matrix

membrane (MMM) doped by various zeolite imidazolate frameworks, *High Perform. Polym.*, 2021, **33**, 309–325, DOI: **10.1177/0954008320952525**.

36 L. Xu, Y. Qin, L. Liu, J. Xiao and Z. Ding, Fabrication of hydrophobic ZIFs based composite membrane with high CO_2 absorption performance, *Korean J. Chem. Eng.*, 2021, **38**, 1032–1042, DOI: **10.1007/s11814-021-0762-z**.

37 X. Zhang, T. Wang, L. Wu and H. Guo, Construction of Ag@ZIF-8/PVDF mixed-matrix ultrafiltration membranes with high separation performance for dye from high-salinity wastewater by microemulsion coupling with blending, *J. Membr. Sci.*, 2023, **670**, 121371, DOI: **10.1016/j.memsci.2023.121371**.

38 S. Yang, N. Xia, M. Li, P. Liu, Y. Wang and L. Qu, Facile synthesis of a zeolitic imidazolate framework-8 with reduced graphene oxide hybrid material as an efficient electrocatalyst for nonenzymatic H_2O_2 sensing, *RSC Adv.*, 2019, **9**, 15217–15223, DOI: **10.1039/c9ra02096a**.

39 P. H. Chang, Y. T. Lee and C. H. Peng, Synthesis and characterization of hybrid metal zeolitic imidazolate framework membrane for efficient H_2/CO_2 gas separation, *Materials*, 2020, **13**, 1–15, DOI: **10.3390/ma13215009**.

40 A. Khan, M. Ali, A. Ilyas, P. Naik, I. F. J. Vankelecom, M. A. Gilani, M. R. Bilad, Z. Sajjad and A. L. Khan, ZIF-67 filled PDMS mixed matrix membranes for recovery of ethanol via pervaporation, *Sep. Purif. Technol.*, 2018, **206**, 50–58, DOI: **10.1016/j.seppur.2018.05.055**.

41 N. Jafari, S. Zeinali and J. Shadmehr, Room temperature resistive gas sensor based on ZIF-8/MWCNT/AgNPs nanocomposite for VOCs detection, *J. Mater. Sci.: Mater. Electron.*, 2019, **30**, 12339–12350, DOI: **10.1007/s10854-019-01592-7**.

42 H. Sun, Z. Magnuson, W. He, W. Zhang, H. Vardhan, X. Han, G. He and S. Ma, PEG@ZIF-8/PVDF nanocomposite membrane for efficient pervaporation desulfurization via a layer-by-layer technology, *ACS Appl. Mater. Interfaces*, 2020, **12**, 20664–20671, DOI: **10.1021/acsami.0c02513**.

43 Y. Rao, F. Ni, Y. Sun, B. Zhu, Z. Zhou and Z. Yao, Efficient recovery of the volatile aroma components from blackberry juice using a ZIF-8/PDMS hybrid membrane, *Sep. Purif. Technol.*, 2020, **230**, 115844, DOI: **10.1016/j.seppur.2019.115844**.

44 P. Kaspar, D. Sobola, K. Částková, R. Dallaev, E. Šťastná, P. Sedlák, A. Knápek, T. Trčka and V. Holcman, Case study of polyvinylidene fluoride doping by carbon nanotubes, *Materials*, 2021, **14**, 1–11, DOI: **10.3390/ma14061428**.

45 X. Qian, N. Li, Q. Wang and S. Ji, Chitosan/graphene oxide mixed matrix membrane with enhanced water permeability for high-salinity water desalination by pervaporation, *Desalination*, 2018, **438**, 83–96, DOI: **10.1016/j.desal.2018.03.031**.

46 R. Castro-Muñoz, Breakthroughs on tailoring pervaporation membranes for water desalination: A review, *Water Res.*, 2020, **187**, 116428, DOI: **10.1016/j.watres.2020.116428**.

47 I. Prihatiningtyas, G. A. Gebreslase and B. Van der Bruggen, Incorporation of Al_2O_3 into cellulose triacetate membranes to enhance the performance of pervaporation for desalination of hypersaline solutions, *Desalination*, 2020, **474**, 114198, DOI: **10.1016/j.desal.2019.114198**.

48 I. Prihatiningtyas, Y. Li, Y. Hartanto, A. Vananroye, N. Coenen and B. Van der Bruggen, Effect of solvent on the morphology and performance of cellulose triacetate membrane/cellulose nanocrystal nanocomposite pervaporation desalination membranes, *Chem. Eng. J.*, 2020, **388**, 124216, DOI: **10.1016/j.cej.2020.124216**.

49 D. A. Reino Olegário da Silva, L. C. Bosmuler Zuge and A. de Paula Scheer, Preparation and characterization of a novel green silica/PVA membrane for water desalination by pervaporation, *Sep. Purif. Technol.*, 2020, **247**, 116852, DOI: **10.1016/j.seppur.2020.116852**.

50 H. Zeng, S. Liu, J. Wang, Y. Li, L. Zhu, M. Xu and C. Wang, Hydrophilic SPEEK/PES composite membrane for pervaporation desalination, *Sep. Purif. Technol.*, 2020, **250**, 117265, DOI: **10.1016/j.seppur.2020.117265**.

51 S. S. Ibrahim, Theoretical study of the effective parameters for direct contact membrane distillation in hollow fiber modules, *Eng. Technol. J.*, 2014, **32**, 2949–2969, **https://uotechnology.edu.iq/tec_magaz/2014/volum322014/No.12.A.2014/Text(8).pdf**.